INTERNATIONAL JOURNAL FOR NUMERICAL METHODS IN FLUIDS
Int. J. Numer. Meth. Fluids 2007; **53**:915–931
Published online 23 August 2006 in Wiley InterScience (www.interscience.wiley.com). DOI: 10.1002/fld.1312

Optimization of heat-transfer rate into time-periodic two-dimensional Stokes flows

J. P. B. Mota[1,*,†], A. J. S. Rodrigo[1] and E. Saatdjian[2]

[1]*Requimte/CQFB, Departamento de Química, Faculdade de Ciências e Tecnologia, Universidade Nova de Lisboa, 2829-516 Caparica, Portugal*
[2]*GDR 681: Chaos Lagrangian 3-D, 2 ave. de la forêt de Haye, BP 160, 54504 Vandœuvre Cédex, France*

SUMMARY

The periodic boundary displacement protocol leading to the optimum wall-to-fluid heat-transfer rate, or to the most efficient mixing rate, in 2-D annular Stokes flows is determined by calculating the steady periodic velocity and temperature fields. To obtain the steady periodic state one usually solves the dynamical system obtained after the spatial coordinates have been discretized. Here, we calculate the steady periodic state using an implicit method based on the discretization of the time coordinate over a period and the asymptotic regime is enforced by the periodicity condition in the computed temperature field. The obtained system of equations is solved using a Newton-type iterative algorithm with invariant Jacobian. At each iteration step, the sparse linearized system is solved using a multi-grid algebraic technique of rapid convergence. From a computational point of view and for the problem considered here, this method is an order of magnitude faster than the one based on a spatial discretization. Copyright © 2006 John Wiley & Sons, Ltd.

Received 8 August 2004; Revised 3 June 2006; Accepted 19 June 2006

KEY WORDS: chaotic advection; Lagrangian turbulence; steady periodic state; periodic modulation; optimization of mixing rate; heat transfer rate

1. INTRODUCTION

Engineers are always looking for methods to increase the heat-transfer rate into fluids in motion. For fluids with low to moderate viscosity the heat-transfer rate into them is usually increased in

*Correspondence to: J. P. B. Mota, Requimte/CQFB, Departamento de Química, Faculdade de Ciências e Tecnologia, Universidade Nova de Lisboa, 2829-516 Caparica, Portugal.
†E-mail: pmota@dq.fct.unl.pt

Contract/grant sponsor: Portuguese Foundation for Science and Technology (FCT/MCES); contract/grant numbers: PRAXIS XXI/BD/18282/98, PRAXIS XXI/BCC/22223/99, POCTI/EME/61713/2004
Contract/grant sponsor: French CNRS

processes by the promotion of turbulence. This is usually done by violent agitation; the impeller shape and its angular velocity are critical parameters there. For highly viscous fluids the situation is different. Although one can in principle also try to promote turbulence, this solution is not viable because it leads to very high pressure drops (and thus high energy costs) and in some cases the stresses created are sufficient to break long molecular chains and degrade the fluid properties. An efficient way to increase the heat transfer rate into viscous fluids is to promote *chaotic advection* or *Lagrangian turbulence* [1–3]. This phenomenon can be described as chaotic particle trajectories (as in turbulence) in a flow dominated by viscous forces. From an Eulerian point of view the flow is periodic; however, from a Lagrangian point of view the flow is chaotic or periodic depending on the initial location of a given material point [4].

In this work we seek to determine how to displace time-periodically the boundaries in 2-D annular Stokes flows so that the heat transfer rate into the fluid is a maximum. This requires the calculation of the steady periodic state in either one of the two geometries discussed in Section 2. There we present the necessary known information and results required to fully understand some of the choices made in this study. The direct numerical method to obtain the steady-periodic temperature profile in the annular regions is discussed in the next section. The method employed here is based on one used to optimize periodic adsorption processes. The results obtained are discussed in Section 4. They show that there is an optimum modulation frequency for which the heat transfer rate into the fluid is a maximum. Other analytical/numerical tools that have been developed for the study of chaotic advection confirm the results obtained here.

2. TWO-DIMENSIONAL FLOW GEOMETRIES

Consider the annular region between eccentric cylinders as shown in Figure 1(a). Two dimensionless parameters are required to completely describe this geometry: the clearance ratio, R_o/R_i, and the eccentricity ratio, $\varepsilon = e/(R_o - R_i)$, where e is the distance between the centres of the two cylinders. The annular region is filled with a highly viscous liquid and the inner and outer cylinders can both rotate at a constant angular velocity. In any geometry, when inertial forces can be neglected,

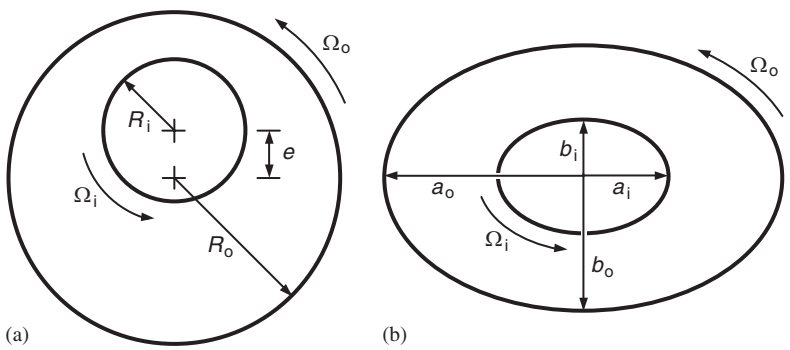

Figure 1. Diagram showing the annular region between: (a) eccentric rotating cylinders; and (b) gliding confocal ellipses. In the latter case the walls glide circumferentially so that the geometry is invariant in time. Ω_i and Ω_o represent the angular velocity of the inner and outer boundaries, respectively.

DOI: 10.1002/fld

the flow field can be obtained by solving the Stokes equations

$$\nabla P = \mu \nabla^2 \mathbf{V}, \quad \nabla \cdot \mathbf{V} = 0 \tag{1}$$

where μ is the fluid viscosity and P is the pressure.

The journal bearing problem described by the geometry of Figure 1(a) is more than a century old and was first studied by Reynolds [5] and Sommerfeld [6]. Jeffery [7] and, later (but with all the expressions for the constants), Ballal and Rivlin [8] obtained the analytical solution in closed form using a bipolar, orthogonal coordinate system. Two other analytical solutions have appeared in the literature: Wannier [9] used a mixed Cartesian-cylindrical non-orthogonal system of coordinates and DiPrima and Stuart [10] used an orthogonal, modified bipolar coordinate system which degenerates into polar coordinates as the eccentricity tends towards zero.

The streamlines obtained using the analytical solution of Ballal and Rivlin [8] are plotted in Figure 2 and they correspond to: (a) outer cylinder rotation, (b) inner cylinder rotation, (c) counter-rotation, and (d) co-rotation. An examination of Figure 2 shows that the flow separates into two

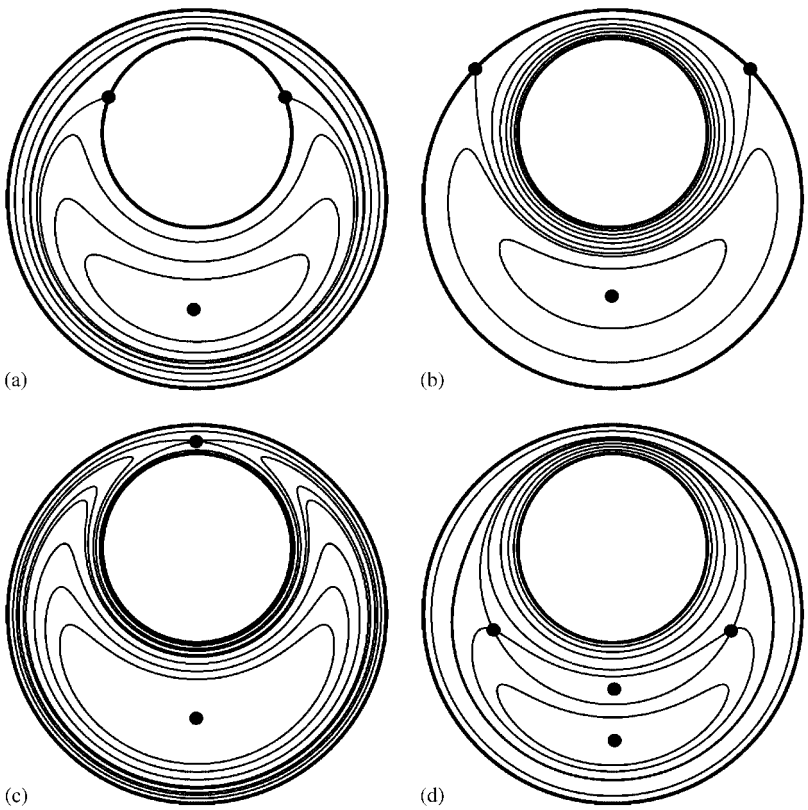

Figure 2. Streamlines between eccentric, rotating cylinders: (a) outer cylinder rotation; (b) inner cylinder rotation; (c) counter-rotation ($\Omega_i/\Omega_o = -2$); and (d) co-rotation ($\Omega_i/\Omega_o = 3$). The geometric parameters are: $R_o/R_i = 2$, $\varepsilon = e/(R_o - R_i) = 0.7$.

DOI: 10.1002/fld

(cases (a) and (b)) or three regions (cases (c) and (d)). Neither case can be considered as a good mixer since fluid in one region remains there and cannot flow into other regions. For all cases the streamlines are symmetrical around an axis passing through the centres of both cylinders, this is a consequence of the reversibility of Stokes flows.

Let us consider the flow topology of the counter-rotation case in more detail. When the cylinders turn in opposite directions there are three flow regions: one turning with the inner cylinder, one turning with the outer cylinder and a vortex zone. Furthermore, a *homoclinic saddle point* appears in the region of minimum gap. Now, it is well known [4] that if a homoclinic saddle point is perturbed (e.g. by continuously varying the angular velocity ratio) then fluid is allowed to flow from one zone to the other and, as we shall see later, this also leads to an enhancement of the heat transfer rate into or out of the fluid.

The plotted solution for co-rotation, shown in Figure 2(d) also shows two saddle points connected by two different streamlines. However, as the angular velocity ratio is varied, the saddle points remain in the same region. Upon perturbation, only fluid in the vicinity of the saddle point can be transported into another region. In the counter-rotating case, by varying the angular velocity ratio over the widest possible range so that the saddle point moves from the inner to the outer boundary, practically all the fluid contained in the annular region can be transported from one region to another.

Because fluid is transported from one flow region into another in the vicinity of a saddle point, one must look for two-dimensional flows exhibiting more of these saddle points. For this reason the flow configuration shown in Figure 1(b) was imagined [11]. It consists of the annular region between two confocal ellipses, the inner and outer boundaries *glide* along their circumference so that the geometry is invariant. Notice that there are two area increases (or decreases) for flow passage per turn in this geometry, while there is only one in the journal bearing flow.

To analyse this flow one must first define an appropriate coordinate system. Elliptical cylindrical coordinates defined by the transformations

$$x = a \cosh u \cos v, \quad y = a \sinh u \sin v, \quad z = z \tag{2}$$

are orthogonal and each boundary is described by a fixed value of the coordinate u. For Stokes flow, and with the boundaries gliding at constant velocity so that the geometry is invariant, the solution of Equation (1) for the velocity vector $\mathbf{V} = (V_u, V_v)$ in elliptical cylindrical coordinates was obtained by Saatdjian *et al.* [11, 12].

In Figure 3 we show streamlines for six different cases of steady boundary motion. As shown in Figure 3(c), when the boundaries move in opposite directions, two *heteroclinic saddle points* joined by two different streamlines appear in the regions of minimum gap. Since transport of fluid from one flow region to another occurs in the vicinity of a disrupted saddle point, one expects that chaotic transport in this flow geometry (with two saddle points) will be greater than in the journal bearing flow.

To *quantify* chaotic mixing/heat transfer into a fluid a very simple experiment can be imagined. Let us assume that the inner and outer boundaries (of any geometry) are at two different temperatures, T_i and T_o, respectively, and that the boundaries are both turning at a constant velocity. The temperature profile in the annular region can be obtained numerically by solving the dimensionless advection-diffusion equation

$$\mathbf{V} \cdot \nabla T = \frac{1}{Pe} \nabla^2 T \tag{3}$$

DOI: 10.1002/fld

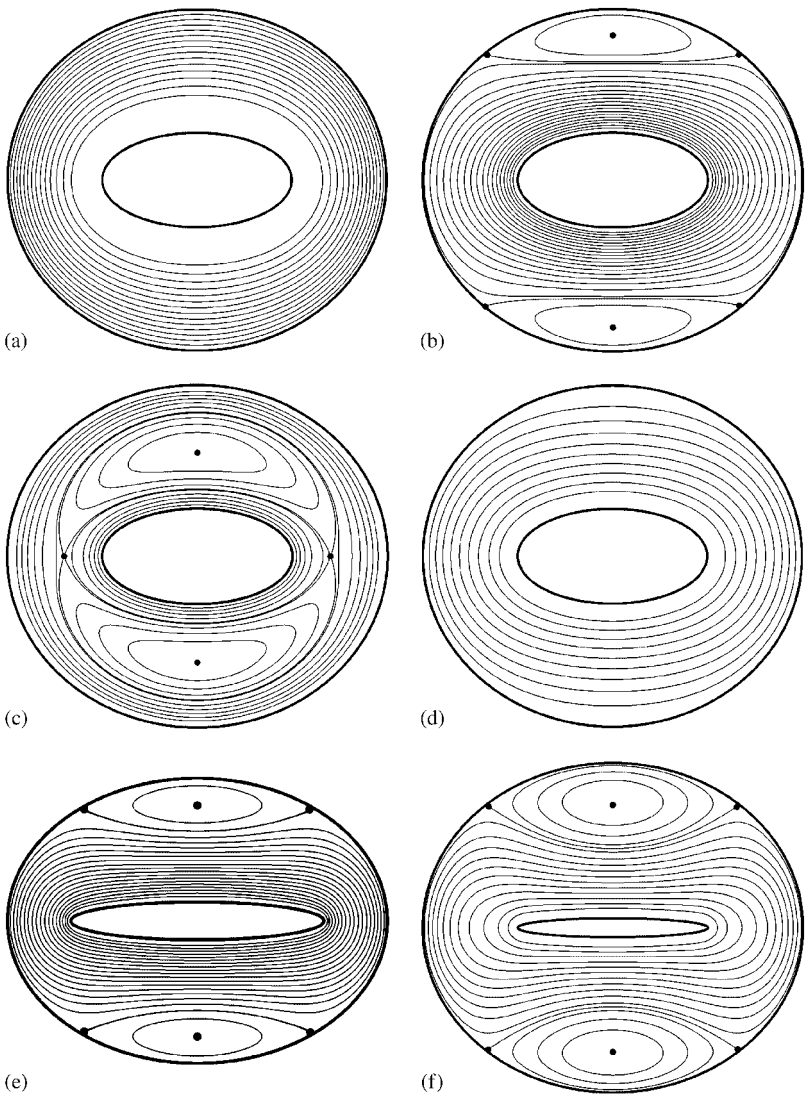

Figure 3. Streamlines for the steady flow between confocal gliding ellipses. The geometrical parameters and the angular velocity ratio are: (a) $a_o/a_i = 2$, $b_i/a_i = 0.5$, $\Omega_i = 0$, $\Omega_o = 3$; (b) $a_o/a_i = 2$, $b_i/a_i = 0.5$, $\Omega_i = 3$, $\Omega_o = 0$; (c) $a_o/a_i = 2$, $b_i/a_i = 0.5$, $\Omega_i/\Omega_o = -3$; (d) $a_o/a_i = 2$, $b_i/a_i = 0.5$, $\Omega_i/\Omega_o = 3$; (e) $a_o/a_i = 1.5$, $b_i/a_i = 0.15$, $\Omega_i/\Omega_o = 200$; and (f) $a_o/a_i = 2$, $b_i/a_i = 0.1$, $\Omega_i/\Omega_o = 500$.

where *Pe* is the Péclet number. After obtaining the steady-state temperature field one can calculate the average Nusselt number which is defined as

$$Nu = \frac{(\text{heat flux})_{\text{convection}}}{(\text{heat flux})_{\text{conduction}}} \tag{4}$$

DOI: 10.1002/fld

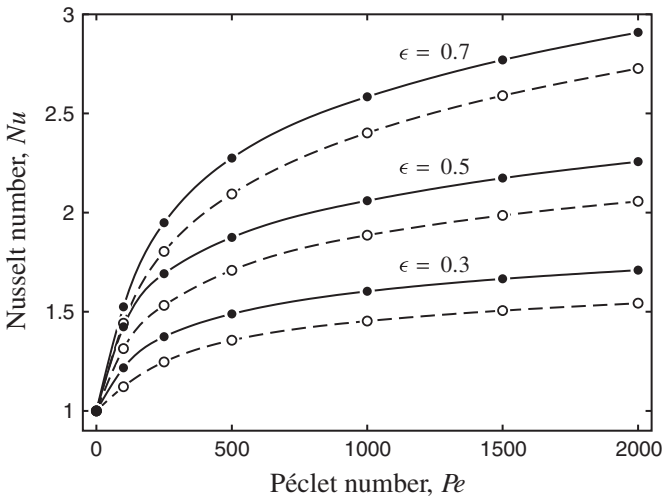

Figure 4. Nusselt number, Nu, as a function of Péclet number, $Pe = 2\pi R_o \Omega_o (R_o - R_i)/\alpha$, for the steady counter-rotating journal bearing flow with $R_o/R_i = 2$. The plot is given for three values of ε and two values of the angular velocity ratio: $\Omega_i/\Omega_o = -1$ (solid circles) and $\Omega_i/\Omega_o = -2$ (open circles).

Using the analytical velocity field and solving the advection-diffusion equation to obtain the temperature field one can calculate the average Nusselt number in the annular region. Figure 4 shows the Nusselt number in the journal bearing as a function of Péclet number for different values of the eccentricity ratio and the angular velocity ratio. The Nusselt number is greater than unity because the circulation zone mixes fluid in it so that the temperature there is practically constant. This leads to a heat-transfer rate increase, as evidenced by the higher temperature gradient at both walls. This is shown in Figure 5 where the radial temperature profile is plotted in the regions of minimum and maximum gap. In Figure 4, as the eccentricity ratio increases, the size of the vortex zone increases so that the heat transfer enhancement by slender recirculation increases. This is also the case when the absolute value of the angular velocity ratio $|\Omega_i/\Omega_o|$ increases.

So far the heat-transfer rate enhancement into the fluid has been due to the formation of a vortex zone. To increase the heat transfer rate even further one must allow fluid to go from one region to the other. One way to do this is to perturb the hyperbolic saddle point, e.g. by varying time-periodically the instantaneous angular velocity ratio of the two cylinders. Another possibility is to allow the inner cylinder to both turn and move [13]. Here, we chose to vary sinusoidally the inner cylinder angular velocity around a mean value $\overline{\Omega}_i$. The modulation protocol is

$$\Omega_i(t) = \overline{\Omega}_i(1 + \delta \sin \omega t) \tag{5}$$

where δ is the amplitude and ω is the modulation frequency. When the cylinders turn in opposite directions, the streamlines show that a saddle point appears in the region of minimum gap, as mentioned earlier. If the angular velocity ratio is increased, the saddle point moves from the inner cylinder towards the outer boundary, but the flow topology remains the same. Obviously, the best modulation protocol is one whose average angular velocity ratio varies over the widest possible

DOI: 10.1002/fld

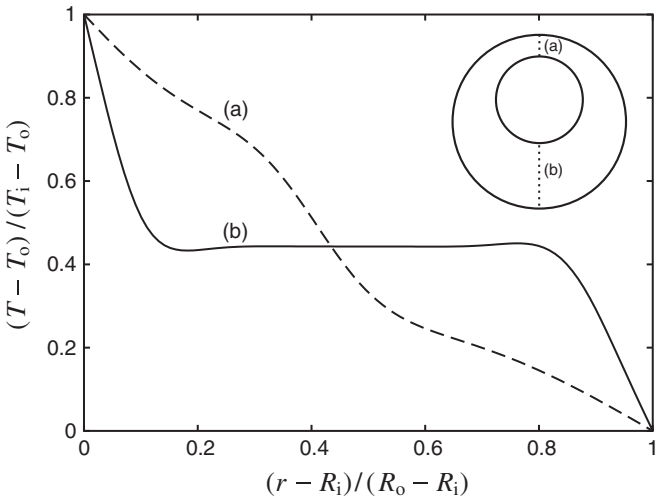

Figure 5. Dimensionless radial temperature distribution in the regions of: (a) minimum; and (b) maximum gap between eccentric, counter-rotating cylinders. The geometric parameters and the angular velocity ratio are: $R_o/R_i = 2$, $\varepsilon = e/(R_o - R_i) = 0.5$, $\Omega_i/\Omega_o = -2$. The Péclet number is $Pe = 2\pi R_o \Omega_o (R_o - R_i)/\alpha = 1000$, where α is the thermal diffusivity of the fluid.

range so that the saddle point moves from the inner boundary to the outer one [14], i.e. the value of $|\overline{\Omega}_i/\Omega_o|$ is large, though Stokes flow conditions must prevail.

However, one must also determine the appropriate modulation frequency so that the heat transfer rate into the fluid is a maximum. To do this one must solve the time-periodic conservation of energy equation,

$$\frac{\partial T}{\partial t} + \mathbf{V} \cdot \nabla T = \frac{1}{Pe} \nabla^2 T \tag{6}$$

to determine the temperature field over a period. The modulation is assumed to be sufficiently slow so that the velocity field $\mathbf{V}(u, v, t)$ is determined by solving the Stokes equations at the instantaneous value of the angular velocity ratio. This can be written mathematically as

$$\mathbf{V}(u, v, t) \approx \mathbf{V}(u, v)|_{\Omega_i(t)/\Omega_o} \tag{7}$$

This assumption is valid as long as the Strouhal number is small, i.e. $Sr = \omega L/V \ll 1$ (V is a characteristic velocity, e.g. $V = \Omega_o R_o$, and L is a characteristic length, say $L = R_o - R_i$).

After a sufficient number of modulation periods, the system reaches a steady periodic state where conditions at the end of the period are the same as those at the beginning. In mathematical terms the steady periodic state can be expressed in the following way:

$$T(u, v, 0) = T(u, v, \tau) \quad \forall u \in (u_i, u_o), \quad v \in (0, 2\pi) \tag{8}$$

where $\tau = 2\pi/\omega$ is the duration of the modulation period.

To measure the heat-transfer rate into the fluid it is convenient to define an instantaneous Nusselt number, which is the ratio of the heat transfer rate in the actual flow to the heat transfer rate if

DOI: 10.1002/fld

the boundaries are motionless (i.e. a pure conduction heat transfer rate):

$$Nu(t) = \frac{u_o - u_i}{T_o - T_i} \int_0^{2\pi} \left(\frac{\partial T}{\partial u} \right)_{u_i, u_o} \mathrm{d}v \tag{9}$$

As the system reaches the steady periodic state, the mean Nusselt number per period,

$$\overline{Nu}(t) = \int_t^{t+\tau} Nu \, \mathrm{d}t' \tag{10}$$

tends asymptotically towards a fixed value, $\overline{Nu}(\infty)$, which must be rendered a maximum.

3. DIRECT METHOD TO OBTAIN THE STEADY PERIODIC STATE

To determine the steady periodic state of a given two-dimensional flow with time-periodic boundary conditions it is usual to replace the spatial derivatives by algebraic equations resulting from a suitable discretization and then to solve the obtained dynamical system [12, 15, 16]. An arbitrary initial condition is chosen and the ordinary differential equations are then integrated until the steady periodic state is established. This methodology based on the 'method of lines' [17, 18] can be very time-consuming if the modulation frequency is high and/or if the fluid conducts heat poorly.

Mathematically, to determine the value of $\overline{Nu}(\infty)$ one must solve numerically Equation (6) for a long period of time, i.e. one must calculate successive values of the average Nusselt number $\overline{Nu}$ at the inner (i) and outer (o) walls,

$$\overline{Nu}_i(k\tau), \quad \overline{Nu}_o(k\tau), \quad k = 0, 1, 2, \ldots \tag{11}$$

until both values are invariant. Calculations are stopped when the following conditions are satisfied:

$$|\overline{Nu}_i((k+1)\tau) - \overline{Nu}_i(k\tau)| < \mathrm{TOL} \quad \text{and} \quad |\overline{Nu}_o((k+1)\tau) - \overline{Nu}_o(k\tau)| < \mathrm{TOL} \tag{12}$$

where TOL is a predefined maximum tolerance value accepted in the calculation of $\overline{Nu}(\infty)$. In theory one must obtain that

$$\overline{Nu}_i(\infty) = \overline{Nu}_o(\infty) = \overline{Nu}(\infty) \tag{13}$$

This condition, however, cannot be verified precisely since all discretization methods involve a given approximation. Nevertheless, values which differ by less than 1% have been reported in the literature [12].

The integration of the equations during a whole period is equivalent to establishing a transformation $\mathscr{H}(\cdot)$ such that, for given initial conditions, one solves for the steady periodic state at the end of the period:

$$T(u, v, \tau) = \mathscr{H}(T(u, v, 0)) \quad \forall u \in (u_i, u_o), \quad v \in (0, 2\pi) \tag{14}$$

DOI: 10.1002/fld

The usual method to determine the steady periodic state can be interpreted as a method to force the periodicity condition through a successive substitution scheme:

$$\begin{cases} T^{[k]}(u, v, \tau) = \mathscr{H}(T^{[k]}(u, v, 0)) \\ T^{[k+1]}(u, v, 0) = T^{[k]}(u, v, \tau) \end{cases} \quad \forall u \in (u_{\mathrm{i}}, u_{\mathrm{o}}), \quad v \in (0, 2\pi), \quad k = 1, 2, \ldots \tag{15}$$

This method has the advantage of correctly simulating the heat transfer dynamics as the steady periodic state is reached. Nevertheless, given the first-order accuracy of this iteration process, a great number of periods is usually necessary to reach the final steady periodic state.

Obtaining the steady periodic state of a given system by a direct method is an important topic in many engineering fields and in applied mechanics. For example, Smith and Westerberg [19] suggested the use of an iterative Newton's method to solve systems of equations of the type

$$\phi(\mathbf{x}, 0) - \mathscr{H}(\phi(\mathbf{x}, 0)) = 0 \tag{16}$$

where ϕ represents the set of dependent variables and $\mathbf{x}$ is the spatial domain. The iteration process begins with three cycles of successive substitution in order to construct a diagonal approximation of the Jacobian system matrix. The matrix inverse is calculated at each step using a formula based on the secant method.

Theoretically the main advantage of Newton-type iterative algorithms is to obtain supralinear convergence rates near the solution. However, in most applications, evidence shows that a satisfactory result is only obtained when one begins and calculates at each step an accurate value of the Jacobian. In practice this implies that the Jacobian must be calculated using finite differences at the first iteration and occasionally in all subsequent ones. In the present case this method is prohibitive given the dimension and the sparse structure of the transformation $\mathscr{H}(\cdot)$. To overcome these difficulties, Croft and LeVan [20] suggested that the Jacobian of Equation (16) be calculated by a method based on the integration of the sensitivity equations

$$\frac{\partial \phi(\mathbf{x}, t)}{\partial \phi(\mathbf{x}, 0)}, \quad t \in (0, \tau) \tag{17}$$

in conjunction with the differential system which models the system dynamics. This can be done by applying Newton's method to the solution of Equation (16), and this guarantees a quadratic convergence rate near the solution if the sensitivity equations are calculated with enough accuracy. The main disadvantage of this method is that the computational time can increase considerably due to the dimension and the sparse nature of the sensitivity matrix. As a rule of thumb, one can state that Newton's method is competitive only if the number of iterations is reduced by a factor of at least two or three orders of magnitude with respect to the method of successive substitution.

In the optimization of periodic adsorption processes, Nilchan and Pantelides [21] recently suggested a method where the spatial and the temporal domains are discretized and the time-periodic boundary condition is directly imposed. The discretization results in a sparse system of algebraic equations, which can be solved numerically to determine directly the steady periodic state. This method was employed in this work.

In practice, the modulation period was divided into n_k time-steps (Figure 6) with duration $\Delta t = \tau / n_k$ and the temperature time derivative $\partial T / \partial t$ was discretized using a second-order

DOI: 10.1002/fld

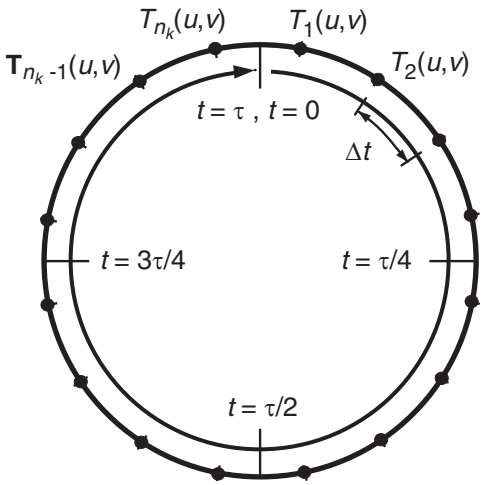

Figure 6. Schematic representation of the circular temporal domain of duration τ, divided into n_k time-steps of length $\Delta t=\tau/n_k$.

backward finite-difference formula:

$$\left.\frac{\partial T(u,v,t)}{\partial t}\right|_{t_k}=\frac{3T(u,v,t_k)-4T(u,v,t_{k-1})+T(u,v,t_{k-2})}{2\Delta t},\quad k=3,\ldots,n_k \tag{18}$$

Imposing the time-periodic boundary condition directly permits us to obtain approximation formulas for $\partial T/\partial t$ for the first two time-steps of the cycle:

$$\begin{aligned}\left.\frac{\partial T(u,v,t)}{\partial t}\right|_{t_1}&=\frac{3T(u,v,t_1)-4T(u,v,t_{n_k})+T(u,v,t_{n_k-1})}{2\Delta t}\\ \left.\frac{\partial T(u,v,t)}{\partial t}\right|_{t_2}&=\frac{3T(u,v,t_2)-4T(u,v,t_1)+T(u,v,t_{n_k})}{2\Delta t}\end{aligned} \tag{19}$$

Briefly, the discretization of the temporal domain substitutes Equation (6) by a system of partial differential equations

$$F_{u,v}(\mathbf{T})=0,\quad \mathbf{T}(u,v)=[T_1(u,v),\ldots,T_{n_k}(u,v)] \tag{20}$$

where only the spatial coordinates appear and where the periodic condition is implicit. In Equation (20), $T_k(u,v)$ represents the thermal field $T(u,v,t_k)$ at time instant t_k.

For simplicity we have adopted a regular spatial grid. The finite-volume method [22] was implemented. The diffusion terms ($\nabla^2 T/Pe$) were approximated by second-order centred finite differences, while the advection terms $\mathbf{V}\cdot\nabla T$ were discretized using the flux-limiter harmonic scheme of van Leer and implemented as suggested by Waterson and Deconinck [23]. For example, assuming that $V_v(u_i, v_{j+1/2}, t_k)>0$ then the flux-limiter scheme for the face value $T(u_i, v_{j+1/2}, t_k)\equiv T_{i,j,k}$

DOI: 10.1002/fld

is implemented as

$$T_{i,j+1/2,k} = T_{i,j,k} + \frac{\max\{0, (T_{i,j+1,k} - T_{i,j,k})(T_{i,j+1,k} - T_{i,j,k})\}}{T_{i,j+1,k} - T_{i,j-1,k}} \tag{21}$$

The flux limiter prevents the appearance of artificial oscillations in the numerical solution when the Péclet number is high. The main drawback is that the formula is non-linear in the interpolated variables.

After spatial discretization, Equation (20) reduces to a sparse system of non-linear algebraic equations

$$F(\mathbf{T}) = 0, \quad \mathbf{T} = [T_{ijk}] \quad (i = 1, \ldots, n_i;\ j = 1, \ldots, n_j;\ k = 1, \ldots, n_k) \tag{22}$$

where T_{ijk} represents the value of the temperature $T(u_i, v_j, t_k)$ in grid point (u_i, v_j) of the domain at time-instant t_k. This algebraic system was solved using a traditional Newton's method:

$$\left(\frac{\partial F(\mathbf{T})}{\partial \mathbf{T}}\right)^{[n]} \Delta\mathbf{T}^{[n+1]} = -F(\mathbf{T}^{[n]}), \quad \mathbf{T}^{[n+1]} = \mathbf{T}^{[n]} + \Delta\mathbf{T}^{[n+1]} \tag{23}$$

where $(\partial F(\mathbf{T})/\partial \mathbf{T})^{[n]}$ is the Jacobian matrix of the system calculated at point $\mathbf{T}^{[n]}$. In a parametric study, it is convenient if the initial estimate of the solution, $\mathbf{T}^{[0]}$, is the final solution obtained for the previous value of the parameter. This procedure guarantees convergence and reduces the total number of iterations.

Notice that for the particular case of Equation (6), the Jacobian depends on $\mathbf{T}$ due to the non-linear discretization of the convective terms using the flux-limiter scheme. To prevent repetitive calculations of the Jacobian without penalizing the convergence of Equation (23), we substituted the original Jacobian with an invariant approximation using a first-order upwind finite-difference discretization of the convective terms. Apart from simplicity, this is the only linear scheme which does not introduce artificial oscillations in the numerical solution for high Péclet numbers independently of grid resolution. The drawback is the excessive smoothness of the solution due to the addition of numerical diffusion. In this case, this drawback is irrelevant because the method is only used to determine the approximate Jacobian. The vector $F(\mathbf{T}^{[n]})$ was calculated using the flux-limiter scheme. In summary, we substituted Equation (23) with the iterative process

$$A\Delta\mathbf{T}^{[n+1]} = -F(\mathbf{T}^{[n]}), \quad \mathbf{T}^{[n+1]} = \mathbf{T}^{[n]} + \Delta\mathbf{T}^{[n+1]} \tag{24}$$

where $A = (\partial F'(\mathbf{T})/\partial \mathbf{T})$ is the invariant matrix of the Jacobian resulting from the discretization of the convective terms using a first-order upwind finite difference formula.

The sparse linear system given by Equation (24) was solved using an implicit alternating-direction method ADI [24], in conjunction with a multi-grid method [25, 26]. Despite the fact that the ADI method eliminates local (high frequency) errors quickly, global errors (low frequency) are reduced at a rate inversely proportional to the grid size. Consequently the propagation of global corrections of the solution, for a great number of control volumes, occurs slowly and during many iterations. Multi-grid methods accelerate the convergence of the linear system through the calculation of corrections at a series of levels with progressively more refined grids. The use of these methods reduces significantly the number of iterations and the total CPU time necessary for the convergence of the solution.

DOI: 10.1002/fld

The multi-grid techniques are based on the principle that the global error (low frequency) which exists in a refined grid can be represented in a less refined grid in the form of a local error (high frequency). With a less refined grid, i.e. with fewer cells, global corrections can be transmitted faster between adjacent grids. Since the cost of the calculations in both CPU time and in employed memory decays exponentially with the use of less refined grids, the global error can be eliminated efficiently. When the primary grid is structured, the associated grids at less refined levels are easier to construct since one only needs to suppress lines at regular intervals.

Basically, the calculation of level corrections with the larger grid requires the transfer of residue from the primary grid at the higher level (restriction), the calculation of corrections and their transfer back to the original grid at the higher level (prolongation). The restriction and the prolongation operators used in this work are based on the additive correction strategy described by Hutchinson and Raithby [27].

4. RESULTS AND DISCUSSION

The method described in the previous section was used to determine the influence of the modulation frequency on the value of $\overline{Nu}(\infty)$ for the two 2-D periodic flows discussed earlier. The grid size employed in both geometries is $40 \times 80 \times 50$ (u, v, t), which gives a time step $\Delta t = \tau/50$. Notice that the time domain extends over a single period of modulation and is independent of the frequency. This is in contrast to the traditional approach of numerical integration over a large number of modulation periods to determine the asymptotic time-periodic solution.

For the journal bearing flow with very small clearance ratios, the values of $\overline{Nu}(\infty)$ that we calculated are almost identical to those calculated by Ghosh *et al*. [15]. This is a first test in order to validate our methodology. For the confocal elliptic geometry, the values obtained were compared with success to those of Saatdjian *et al.* [12]. In other cases, we compared our results to those obtained by integrating the dynamical system using the method-of-lines approach. In all cases the difference between the values at each boundary was less than 1%. One must note that the method employed here to obtain the steady periodic state directly, with as initial estimate the periodic thermal field obtained at a neighbouring frequency value, was an order of magnitude faster than the traditional method.

Figure 7 shows the percentage increase in the value of $\overline{Nu}(\infty)$ as a function of ω with respect to the value obtained with no modulation of Ω_i, for the journal bearing flow with $R_o/R_i = 2$ and $Pe = 1000$. For each of the three values of the eccentricity ratio ε, the two curves plotted are for values of $\overline{\Omega}_i/\Omega_o = -1$ and -1.5. In this flow, a compromise must be found in the choice of the eccentricity ratio ε. For small values of ε the vortex zone is small and the heat transfer rate increase is thus also small because it is proportional to the size of the vortex. If the inner boundary is correctly modulated one can see that the increase of the heat transfer rate is of about 10%.

When the value of ε is high, the heat transfer rate increase due to the vortex is high. Modulating the inner cylinder velocity can lead to a slight decrease of the heat transfer rate. For this reason Kaper and Wiggins [14] concluded that the best gains are obtained for a small value of ε and an angular velocity protocol which varies over a very wide range.

Figure 8 shows curves similar to those of Figure 7, for the flow between confocal ellipses defined by $a_o/a_i = 2$ and $Pe = 1000$. Each curve shows the dependence of $\overline{Nu}(\infty)$ with ω for three values of the inner ellipse eccentricity ε and two values of the average angular velocity ratio. In this geometry the gain obtained by an appropriate modulation of the inner ellipse angular velocity is significant and can reach 40% when the inner ellipse eccentricity is small.

DOI: 10.1002/fld

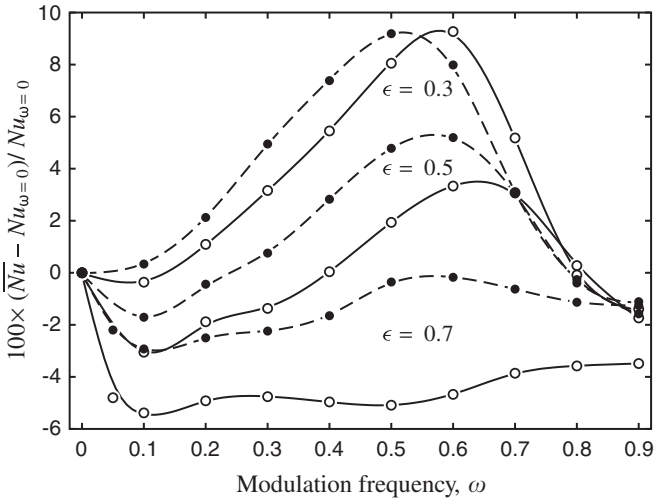

Figure 7. Percent increase of $\overline{Nu}(\infty)$ as a function of ω for the journal bearing flow defined by $R_o/R_i = 2$ and Péclet number $Pe = 2\pi R_o\Omega_o(R_o - R_i)/\alpha = 1000$. The angular velocity modulation of the inner cylinder is $\Omega_i(t) = \overline{\Omega}_i(1 + 0.9\sin\omega t)$. The figure shows the dependence of $\overline{Nu}(\infty)$ with ω for three values of $\varepsilon = e/(R_o - R_i)$ and two values of the average angular velocity: $\overline{\Omega}_i/\Omega_o = -1$ (filled circles) and $\overline{\Omega}_i/\Omega_o = -1.5$ (open cylinders). The lines were obtained by interpolation of the simulation results.

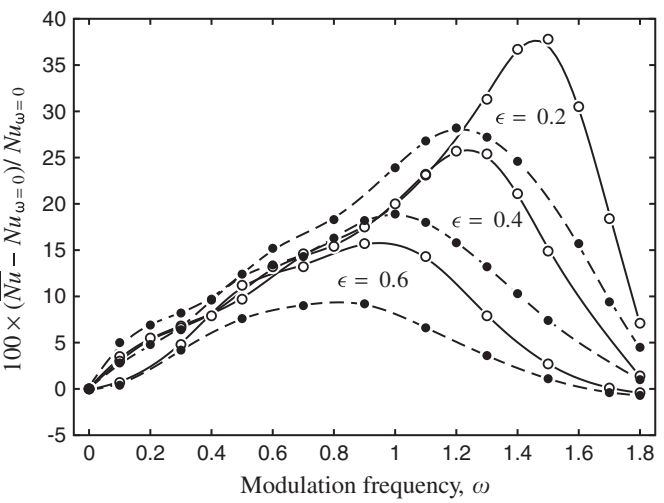

Figure 8. Percent increase of $\overline{Nu}(\infty)$ as a function of ω for the flow between confocal ellipses defined by $a_o/a_i = 2$ and Péclet number $Pe = \Gamma_o\Omega_o(a_o - a_i)/\alpha = 1000$, where Γ_o is the perimeter of the outer ellipse. The inner ellipse angular velocity modulation is $\Omega_i(t) = \overline{\Omega}_i(1 + 0.9\sin\omega t)$. The figure shows the dependence of $\overline{Nu}(\infty)$ with ω for three values of $\varepsilon = b_i/a_i$ and two values of the average angular velocity ratio: $\overline{\Omega}_i/\Omega_o = -1$ (filled circles) and $\overline{\Omega}_i/\Omega_o = -2$ (open circles). The lines were obtained by interpolation of simulation values.

DOI: 10.1002/fld

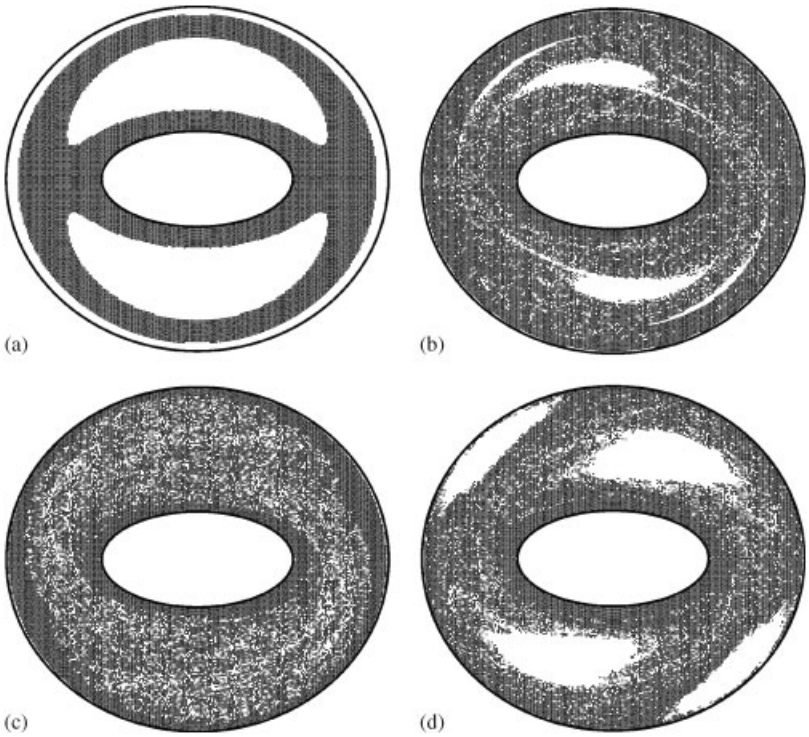

Figure 9. Stretching distribution for the 2-D periodic flow between confocal ellipses. The geometric parameters are: $a_o/a_i = 2$ and $b_i/a_i = 0.5$. The outer ellipse angular velocity is $\Omega_i(t) = \overline{\Omega_i}(1 + 0.9 \sin \omega t)$, with a mean value $\overline{\Omega_i}/\Omega_o = -2$. Black dots indicate the initial position of the particles which stretch more than a critical value $\log_{10} \lambda_c = 10$. The dimensionless modulation frequency ω/Ω_o, for each case is: (a) 0 (without modulation); (b) 16/30; (c) 32/30 (optimum frequency); and (d) 64/30.

The existence of an optimum modulation is corroborated graphically by calculating the stretching field. The stretching distribution is directly proportional to the mixing intensity of a material point in each region of the flow. Material points subject to high stretching rates correspond to regions with good micro-mixing and vice versa. The first stretching calculations for the journal bearing flow were done by Swanson and Ottino [28], who used a discontinuous angular velocity protocol.

To determine the stretching field in the flow between confocal ellipses, a large number of tracer particles was evenly distributed over the whole annular space. The stretching vector $\mathbf{l}$ associated with each particle was then monitored during 30 turns of the outer wall. To calculate the total cumulative stretching of each particle an initial unit stretching vector, $\mathbf{l}_0 \equiv [\mathbf{l}_\alpha, \mathbf{l}_\beta]_0 = [\sqrt{1/2}, \sqrt{1/2}]$, was assigned to it and integrated

$$d\mathbf{l}/dt = (\nabla \mathbf{v})^{\mathrm{T}} \cdot \mathbf{l} \tag{25}$$

as the particle was transported by the flow. The total stretching accumulated per particle is defined as $\lambda = \|\mathbf{l}\|/\|\mathbf{l}_0\|$. It should be pointed out that these calculations are considerably more time consuming than the solution of the steady periodic heat-transfer problem using the full discretization method.

DOI: 10.1002/fld

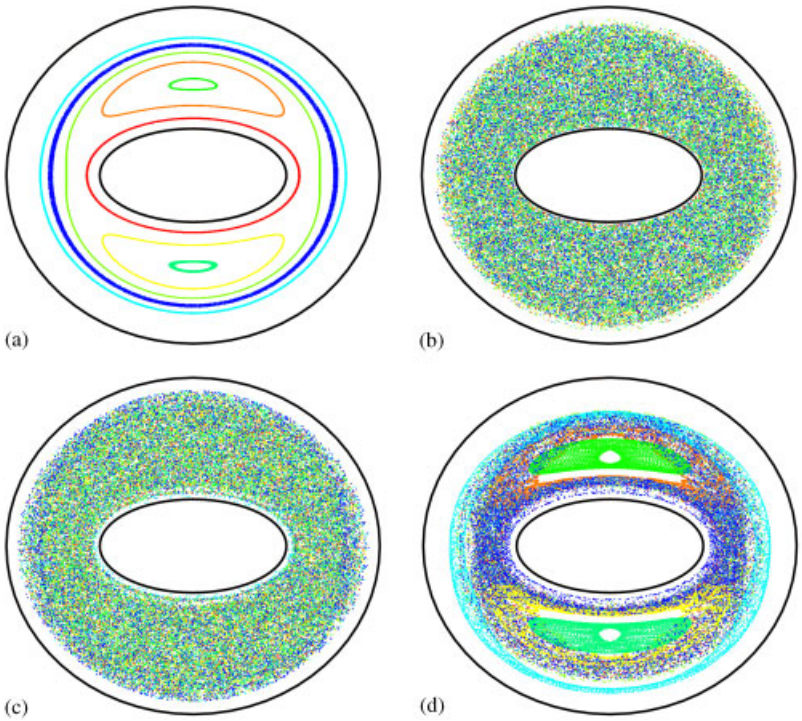

Figure 10. Poincaré sections for the 2-D periodic flow between confocal ellipses, obtained by recording the position of a material point at the end of each full turn of the outer ellipse for six different initial conditions and 6000 iterations. The geometric parameters are: $a_o/a_i = 2$ and $b_i/a_i = 0.5$. The outer ellipse angular velocity is $\Omega_i(t) = \overline{\Omega_i}(1 + 0.9 \sin \omega t)$, with a mean value $\overline{\Omega_i}/\Omega_o = -2$. The dimensionless modulation frequency ω/Ω_o, for each case is: (a) 0 (without modulation); (b) 16/30; (c) 32/30 (optimum frequency); and (d) 64/30.

Figure 9 shows a monochrome plot of the stretching field for four values of the modulation frequency ω. The values of ω were chosen so that we could compare with Figure 8 and correspond to four distinct situations: (a) without any modulation, (b) low frequency, (c) optimum frequency, and (d) high frequency. The tracer particles which have high stretching ($\log_{10} \lambda > 10$) are plotted in black at their initial position while particles which have low stretching ($\log_{10} \lambda < 10$) are plotted in white. In all plots the same cut-off value ($\log_{10} \lambda_c = 10$) was employed. In agreement with other authors [28], the plots were found to be relatively insensitive to the choice of cut-off value λ_c. One must note that for the optimum frequency practically the whole annular region is covered by high stretching zones. This analysis tool shows the relationship which exists between mixing rate and heat transfer rate for this type of two-dimensional flow.

Finally, Poincaré sections are plotted in Figure 10 for the same four cases of Figure 9. A Poincaré section records the position of an arbitrary initial condition at the end of each period. To obtain the plots shown in Figure 10, six initial conditions were chosen initially and their positions at the end of each period were recorded, the program was run for 1000 periods. For two-dimensional chaotic

DOI: 10.1002/fld

flows, Poincaré sections show the regions where tracer will never go. If the initial condition is initially on a chaotic region, the position at the end of each period will change each time. If the initial condition is placed in a regular region it will follow a close orbit depending on the period of the orbit. Although very useful in determining regular and chaotic regions, Poincaré sections do not give an indication of mixing rate. Nevertheless, one must note the similarity between the plots of the Poincaré sections in Figure 10 and the stretching distributions displayed in Figure 9.

5. CONCLUSIONS

The steady periodic solution of the conservation equations in two-dimensional periodic flows was obtained numerically. The direct method employed to obtain the steady periodic fields is computationally more efficient, by an order of magnitude, than the integration of the energy equation. The wall-to-fluid heat-transfer rate was determined by calculating an average Nusselt number per period. This parameter depends on the modulation frequency and was determined for two different flows, the journal bearing flow and the flow between confocal gliding ellipses. For each flow there is an optimum modulation frequency for which the Nusselt number is a maximum, this also corresponds to conditions where mixing by chaotic advection is most efficient. Two other qualitative tools, stretching calculations and Poincaré sections confirm the results obtained above.

ACKNOWLEDGEMENTS

This work was supported by the Portuguese Foundation for Science and Technology (FCT/MCES) through Grants PRAXIS XXI/BD/18282/98, PRAXIS XXI/BCC/22223/99, and POCTI/EME/61713/2004, and the French CNRS, Dépt. Sciences pour l'Ingénieur.

REFERENCES

1. Aref H. Stirring by chaotic advection. *Journal of Fluid Mechanics* 1984; **143**:1–21.
2. Ottino JM. Mixing, chaotic advection and turbulence. *Annual Review of Fluid Mechanics* 1990; **22**:207–253.
3. Aref H. The development of chaotic advection. *Physics of Fluids* 2002; **14**:1315–1325.
4. Ottino JM. *The Kinematics of Mixing*: *Stretching*, *Chaos and Transport*. Cambridge University Press: Cambridge, 1989.
5. Reynolds O. On the theory of lubrication and its application to M. Beauchamp Tower's experiments. *Philosophical Transactions of the Royal Society of London*, *Series A* 1886; **177**:157–234.
6. Sommerfeld A. Zur hydrodynamischen theorie der schmiermittelreibung. *Zeitschrift fur Mathematik und Physik* 1904; **50**:97–155.
7. Jeffery GB. The rotation of two cylinders in a viscous liquid. *Philosophical Transactions of Royal Society of London Series A* 1922; **101**:169–174.
8. Ballal BY, Rivlin RS. Flow of a Newtonian fluid between eccentric, rotating cylinders: inertial effects. *Archives for Rational Mechanics and Analysis* 1976; **62**:237–294.
9. Wannier GH. A contribution to the hydrodynamics of lubrication. *Quarterly of Applied Mathematics* 1950; **8**:1–32.
10. DiPrima RC, Stuart JT. Flow between eccentric rotating cylinders. *ASME Journal of Lubrication Technology* 1972; **94**:266–274.
11. Saatdjian E, Midoux N, André JC. On the solution of Stokes equations between confocal ellipses. *Physics of Fluids* 1994; **6**:3833–3846.
12. Saatdjian E, Midoux N, Chassaing MI, Leprévost JC, André JC. Chaotic mixing and heat transfer between confocal ellipses. *Physics of Fluids* 1996; **8**:677–691.
13. Finn MD, Cox SM. Stokes flow in a mixer with changing geometry. *Journal of Engineering Mathematics* 2001; **41**:75–99.

DOI: 10.1002/fld

14. Kaper T, Wiggins S. An analytical study of transport in Stokes flows exhibiting large-scale chaos in the eccentric journal bearing. *Journal of Fluid Mechanics* 1993; **253**:211–243.
15. Ghosh S, Chang HC, Sen M. Heat transfer enhancement due to slender recirculation and chaotic transport between counter-rotating eccentric cylinders. *Journal of Fluid Mechanics* 1992; **238**:119–154.
16. Lefevre A, Mota JPB, Rodrigo AJS, Saatdjian E. Chaotic advection and heat transfer enhancement in Stokes flows. *International Journal of Heat and Fluid Flow* 2003; **24**:310–321.
17. Carver MB. Method of lines solution of differential equations—fundamental principles and recent extensions. In *Foundations of Computer-Aided Process Design*, Mah RSH, Seider WD (eds). Engineering Foundation: New York, New Hampshire, 1981; 369–402.
18. Schiesser WE. *The Numerical Method of Lines*. Academic Press: New York, 1991.
19. Smith IV OJ, Westerberg AW. The optimal design of pressure swing adsorption processes. *Chemical Engineering Science* 1991; **46**:2967–2976.
20. Croft DT, LeVan MD. Periodic states of adsorption cycles—I. Direct determination and stability. *Chemical Engineering Science* 1994; **49**:1821–1829.
21. Nilchan S, Pantelides CC. On the optimisation of periodic adsorption processes. *Adsorption* 1998; **4**:113–147.
22. Patankar SV. *Numerical Heat Transfer and Fluid Flow*. McGraw-Hill: New York, 1980.
23. Waterson NP, Deconinck H. A unified approach to the design and application of bounded higher-order convection schemes. *Numerical Methods in Laminar and Turbulent Flow*, Taylor C, Durbetaki P (eds), vol. 9. Pineridge Press: Swansea, 1995; 203–214.
24. Wachpress SL. *Iterative Solution of Elliptic Systems*. Prentice-Hall: Englewood Cliffs, NJ, 1966.
25. Briggs WL, Henson VE, McCormick SF. *A Multigrid Tutorial* (2nd edn). SIAM: Philadelphia, PA, 2000.
26. Trottenberg U, Oosterlee CW, Schuller A. *Multigrid*: *Basics*, *Parallelism and Adaptivity*. Academic: San Diego, CA, 2000.
27. Hutchinson BR, Raithby GD. A multigrid method based on the additive correction strategy. *Numerical Heat Transfer* 1986; **9**:511–537.
28. Swanson PD, Ottino JM. A comparative computational and experimental study of chaotic mixing of viscous fluids. *Journal of Fluid Mechanics* 1990; **213**:227–249.

DOI: 10.1002/fld